Transverse Instability of Bubbles in Viscoelastic Channel Flows

Matthew T. Sullivan
Schlumberger Doll Research, 1 Hampshire Street, Cambridge, Massachusetts, USA
School of Engineering and Applied Sciences, Harvard University, 29 Oxford Street, Cambridge, Massachusetts, USA

Karina Moore
Norfolk State University, Norfolk, Virginia, USA

Howard A. Stone
School of Engineering and Applied Sciences, Harvard University, 29 Oxford Street, Cambridge, Massachusetts, USA
(Received 31 December 2007; published 12 December 2008)

The trajectory of a stream of bubbles is measured in a microfluidic pressure-driven flow. For Newtonian fluids with or without surfactants, or viscoelastic fluids without surfactants, the bubbles maintain stable positions equally spaced along the channel center line. However, for viscoelastic fluids with surfactant, a transverse instability is observed, which has the characteristics of a linear instability, whose growth rate increases with the speed of the flow. The results are shown to be consistent with the action of shear-induced normal stresses in the fluid, where the magnitude increases with shear rate and so is augmented by surfactants that make the interface rigid.

DOI: 10.1103/PhysRevLett.101.244503 PACS numbers: 47.50.−d, 47.61.Jd

Microfluidic methods are useful for the control and manipulation of small quantities of fluid. As the use of such techniques expands to include non-Newtonian materials, understanding the interplay of small length scales and nontrivial rheology becomes increasingly important [1]. In addition, non-Newtonian fluids offer desirable flow characteristics at low Reynolds numbers, such as enhanced mixing [2] or directional switching of distinct streams [3], which may not be available with Newtonian fluids. Moreover, the possible dynamical responses are expanded when multiphase flows are considered, such as particle suspensions, foams, and emulsions.

In this Letter, we describe an instability during the flow of bubbles through microfluidic channels. The instability depends on the rheological properties of the fluid, the properties of the gas-liquid interface, and the geometry of the microfluidic channel. Such an instability is indicative of the interplay between rheology and geometry that will be of increasing importance as microfluidic devices are used with a wider range of fluids.

For neutrally buoyant symmetrical rigid particles in rectilinear flows at low Reynolds numbers, there is no cross-streamline migration in Newtonian fluids and any such drift is due either to fluid or particle inertia [4–6] or fluid rheology [7–9]. In viscoelastic fluids, particles small compared to the channel dimensions drift toward the region of lowest shear, which for a pressure-driven flow is the center of the channel. This result is explained qualitatively by viscoelastic forces from the undisturbed flow acting on the particle. For large rigid particles [10–12], a reversal of this effect is observed and the particles drift toward the wall, where the shear rate is highest.

Unlike solid particles, bubbles and droplets show migration even at low Reynolds numbers in Newtonian fluids [13–17]. Again, migration is toward the region of lowest shear and can be explained by nonlinearities associated with the deformation of the fluid-fluid interface. Similar behavior is seen for droplets suspended in non-Newtonian fluids, with both interfacial and viscoelastic forces contributing to deflection [18]. In some cases, an oscillation in the position of bubbles is observed as a result of hydrodynamic interactions between bubbles [19].

Microfluidic flow-focusing devices (Fig. 1) allow for the controllable formation of monodisperse bubbles [20]. We fabricate flow-focusing devices in PDMS using standard soft-lithography techniques. As our focus is on the behavior of bubbles as they travel through the device, the channel continues unperturbed for 4 cm downstream from the flow-focusing junction. This design allows ample length to

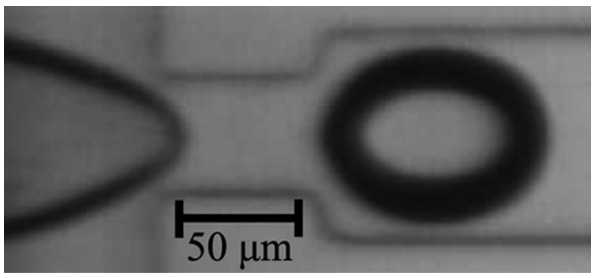

FIG. 1. Typical flow-focusing junction used in these experiments. Channel cross sections are rectangular, 40 μm × 100 μm. The bubble shown is typical of those observed in experiments. For bubble diameters larger than the channel height, the bubble is squashed in the third dimension.

observe any instabilities in the transverse position and bubble spacing along the channel.

Air is used as the gas phase and the pressure is controlled by a regulator. As the continuous phase, which is controlled by a syringe pump, we use solutions of 10^6 molecular weight (MW) polyethylene oxide (PEO) in water-glycerol mixtures. Such solutions are viscoelastic and exhibit both shear thinning viscosity and a normal stress difference. Rheological measurements including normal stresses are performed using a TA Instruments AR-G2 stress-controlled rheometer. The concentration of the solutions ranges from zero to 1.5% PEO by weight. In addition to polymer, varying amounts of Tween 20 are added as a surfactant, with concentrations ranging from zero to 1% by weight (CMC $\approx 10^{-2}$% by weight). As in the Newtonian case [21], we make monodisperse, evenly separated bubbles.

Bubble formation is qualitatively similar in Newtonian and viscoelastic solutions. There is a striking difference, however, in the behavior as the bubbles propagate along the channel. In Newtonian fluids [Fig. 2(a)], with or without surfactant, bubbles travel in the center of the channel and show no transverse velocity component. Similarly, in surfactant-free viscoelastic solutions [Fig. 2(b)], the bubbles remain in the center of the channel. In viscoelastic solutions with surfactant [Fig. 2(c)], however, we observe a transverse instability and bubbles migrate to the channel wall. Cross-stream migration of bubbles in flow has been found in previous experiments [13,17], where bubbles were observed to move toward the center of the channel. Those results explain why bubbles maintain their position at the center of the channel in both Newtonian and surfactant-free polymeric solutions, but do not explain the migration of bubbles toward the wall when both polymer and surfactant are present.

We use a high-speed video camera and image analysis software to measure the positions of the bubbles as a function of time. From the position data, the deviation y_d in the trajectory away from the center line can be calculated. The effects of surfactant and polymer concentration on the deflected trajectories can be quantified by measuring the distance bubbles must travel until they are deflected half way to the channel wall (Fig. 3). Near the center of the channel, there is a linear relationship between the transverse velocity and the center line deviation (Fig. 4). This feature is characteristic of a linear instability—once the bubble is slightly perturbed from the unstable equilibrium in the channel center, the force continues to move the bubble toward the wall. We can quantify the instability by the linear growth rate σ in this central region, i.e., $dy_d/dt = \sigma y_d$.

The transverse instability can be understood in terms of the force resulting from a small displacement from the center of the channel. As the center is an unstable position, we expect that such a force must be larger on the side of the bubble that is further from the wall. Viscoelastic fluids undergoing shear flow show two principle differences in their flow behavior from Newtonian fluids—shear-rate dependence of viscosity and normal stress differences. The shear-rate dependent viscosity will affect fluid flow

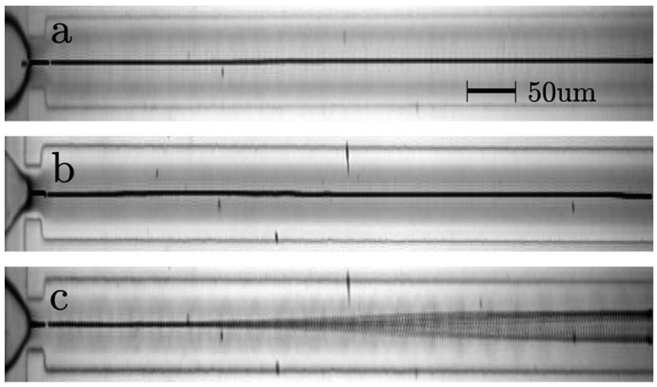

FIG. 2. Plot (dark lines) of the detected center of mass of all bubbles during a flow experiment. (a) For Newtonian solutions, with or without surfactant, bubbles remain in the center of the channel. (b) In a 0.5 wt% 10^6 MW PEO solution without surfactant, bubbles have a similar centered trajectory. No significant deviations from this centered path are observed over the 4 cm length of the device for either (a) or (b). (c) With 0.1 wt % Tween 20 in a solution otherwise identical to (b), bubbles drift from the center to the wall. For sufficiently separated bubbles, motion to either wall is equally probable. All images show an area that is 125 μm $\times$ 3000 μm.

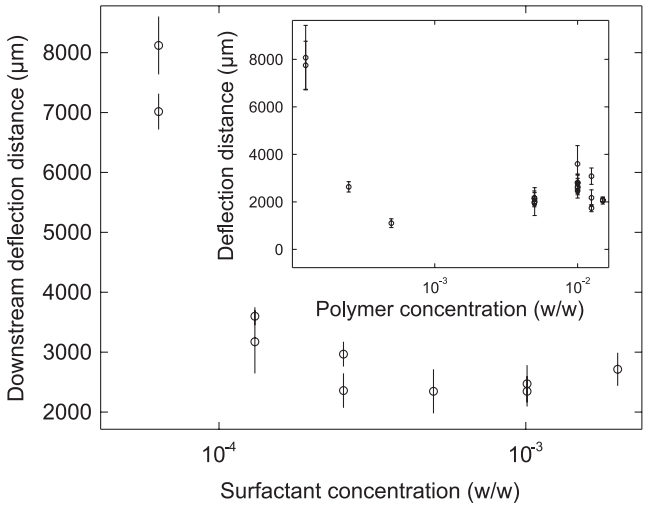

FIG. 3. Average distance downstream before a bubble migrates half the distance to the wall for a variety of Tween 20 concentrations and 1 wt % 10^6 MW PEO. Below 10^{-5} wt% surfactant, no deflection is observed in the 4 cm long channel. At low surfactant concentrations ($\approx 6 \times 10^{-4}$ wt%), the instability is weak and the bubbles are slow to reach the wall. Similar results for polymer concentration in 0.1 wt% Tween are presented in the inset. In the absence of either surfactant or polymer, no deflection is observed.

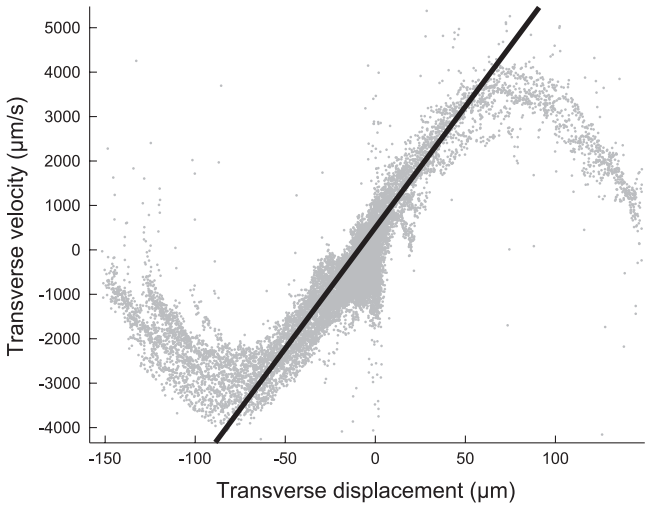

FIG. 4. Transverse bubble velocities dy_d/dt plotted against transverse displacement y_d. The results exhibit a linear relation for small displacements from the center. A fit to this linear region yields a growth rate σ for the transverse instability. The deflection becomes nonlinear as the wall is approached.

around the bubble and contribute to a deviation in the isotropic pressure of the fluid. If the bubble shape is fore-aft symmetric, as observed in our experiments, the requirement of equal pressure drop across the bubble leads to an antisymmetric stress difference on the bubble interface. When integrated, the antisymmetric stress difference yields no net transverse force and thus does not contribute to an instability. Elastic normal stress differences, however, are symmetric about a bubble with a fore-aft symmetric shape and such stresses can lead to a net force on the bubble. For this reason, we focus only on the normal stress contributions at the bubble interface.

The elastic normal stress τ_{yy} along the transverse direction y varies with the local shear rate $\dot{\gamma}$, which we approximate as $\tau_{yy} = N|\dot{\gamma}|^{2n}$, where N and n are properties of the fluid. For the PEO solutions used in our study, n was approximately $1/2$. At a clean gas-liquid interface, the shear rate is zero, and there will be no elastic normal stress acting on the bubble. Surfactant rigidifies the air-liquid interface, which produces local shear in the liquid. This effect, combined with the shear-rate dependence of the elastic normal stress, rationalizes the surfactant dependence of the instability (Fig. 3). At low surfactant concentrations, the interface is nearly stress free, and the normal stresses are small, which leads to no deflection. As the surfactant concentration increases, the interface becomes more rigid and normal stresses provide a net force on the bubble.

To understand the viscoelastic origin of this effect, we estimate the shear rates on the rigid bubble surface. For bubbles that are large in comparison to the gap between the bubble and the channel wall, we make a two-dimensional lubrication approximation to calculate the flow through each side. If we neglect the shear rate dependence of the fluid viscosity and approximate the bubble-wall separation for a bubble of radius a and minimum distance h_s as $h(x) = h_s(1 + x^2/2ah_s)$, the velocity in the channel with a net flow q_s is given by

$$u(x, y) = \frac{6}{h^3}\left(q_s - \frac{u_b h}{2}\right)y(h - y) + u_b\left(1 - \frac{y}{h}\right). \quad (1)$$

From the velocity, we can calculate the shear rate at the bubble surface $\dot{\gamma}$, normal stress τ_{yy}, and total pressure drop, ΔP. Estimating the total force on the bubble as the normal stress at closest approach multiplied by the area at closet approach $\sqrt{2ah_s}$, yields

$$F = N\left(\frac{2u_b}{h_s} + \frac{2\sqrt{2h_s}\Delta P}{3\pi\eta\sqrt{a}}\right)^{2n}\sqrt{2ah_s}. \quad (2)$$

Measurements indicate the bubble velocity is nearly equal to that of the fluid—suggesting that the total fluid flow rate $q_T + q_B = 0$, where subscripts T and B indicate flow rates along the top and bottom channels, respectively. For a bubble with $h_T - h_B = \delta h_0$, the net force per unit depth on the bubble, $F = F_T - F_B$, can then be calculated and expanded for small δ as

$$F_T = (1 + 8n)N(2u_b/h_0)^{2n}\sqrt{2ah_0}\delta. \quad (3)$$

This force is directed toward the near wall, creating a linear instability. This prediction is consistent with force measurements on rigid objects in viscoelastic flow [10,11], where the force observed was toward the near wall.

To compare to growth rate measurements, we calculate the drift velocity. The force required to move a bubble with velocity dy_d/dt toward the wall in a fluid with viscosity η is approximately

$$F = 12\sqrt{2}\eta\left(\frac{a}{h_0}\right)^3\frac{dy_d}{dt}. \quad (4)$$

Equating these forces and recalling $y_d = h_0\delta$ yields

$$\frac{dy_d}{dt} = \frac{(1 + 8n)}{12}\frac{N}{\eta}\left(\frac{2u_b}{h_0}\right)^{2n}\frac{h_0}{a}y_d. \quad (5)$$

This model suggests that for a given polymer and surfactant concentration an increase in the bubble velocity leads to an increased instability growth rate. Measurements of the relative deflection velocity $\sigma h_0 = (dy_d/dt)/\delta$ versus bubble velocity u_b, Fig. 5(a), confirm this trend over a wide range of polymer and surfactant concentrations. For a linear variation in normal stress with shear rate, or $n = 1/2$, the growth rate becomes $\sigma h_0 = 5/6(u_b h_0/a)N/\eta$. The growth rate normalized by bubble velocity, Fig. 5(a) (inset), shows a linear dependence on initial wall separation, as predicted. Larger initial wall separations, corresponding to smaller bubbles, deviate from this trend. This response is to be expected as the approximation of two-dimensional flow ceases to be valid for these smaller

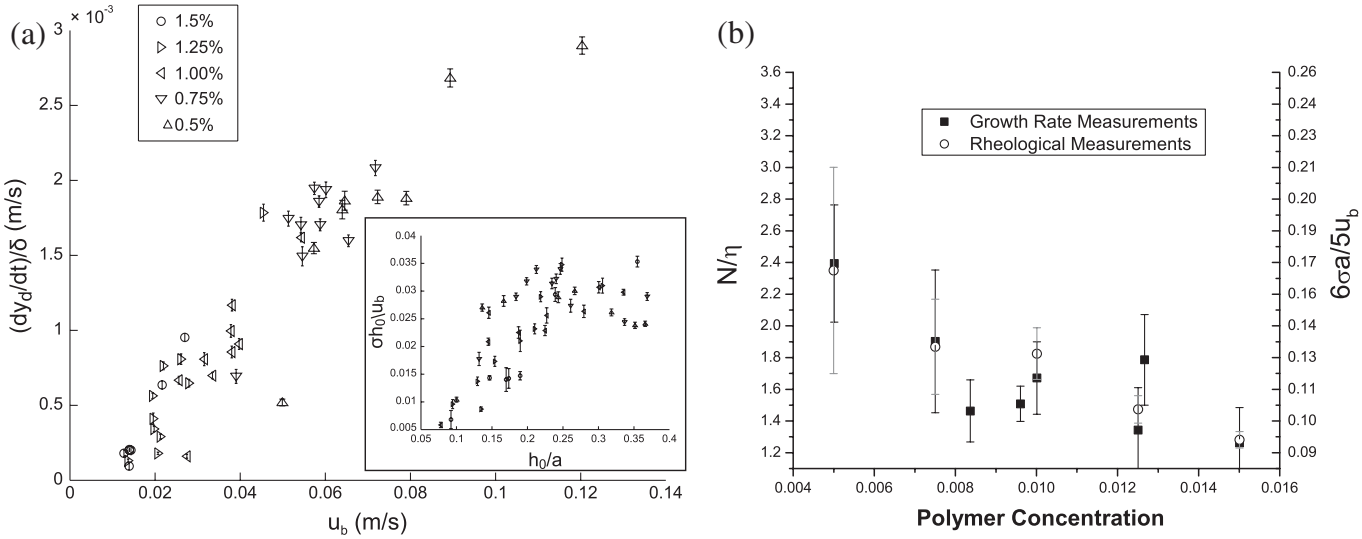

FIG. 5. (a) Instability growth versus bubble velocity for a 0.5 wt% 10^6 MW PEO and 0.1 wt% Tween 20 solutions. The growth rate increases roughly linearly with bubble velocity, which suggests that the normal force scales linearly with shear rate. Normalizing the deflection velocity by the bubble velocity, the scaling of growth rate against wall separation can be measured (inset). For small separations, the variation is approximately linear as expected. The scaling breaks down at large wall separations, corresponding to small bubble diameters. (b) A lubrication model predicts $6\sigma a/5u_b = N/\eta$. Direct comparison of these quantities, taken from deflection and rheological measurements, respectively, shows qualitative agreement.

bubbles. A final test of the model is to compare predictions based on rheological measurements with the observed growth rates [Fig. 5(b)]. The model overpredicts the strength of the effect by a factor of 14, but the trend with polymer concentration is reproduced.

The behavior of bubbles in viscoelastic fluids depends both on the nature of the fluid and the properties of the interface. For surfactant-laden bubbles in viscoelastic fluids, we have shown that both the elastic normal stress of flow and surface properties of the bubble combine to produce a transverse instability. Without surfactant, the interface is stress free and generates no normal stress differences. Only when there is sufficient surfactant can normal stresses be generated to trigger this transverse instability. As microfluidic studies expand to include a wider range of multiphase materials, we expect that the viscoelastic properties and possible instabilities will become more relevant to the operation of microfluidic devices.

We thank the NSF via the Harvard MRSEC (DMR-0213805) and Schlumberger for support of this research and D. Angelescu for helpful conversations.

[1] L. E. Rodd, T. P. Scott, D. V. Boger, J. J. Cooper-White, and G. H. McKinley, J. Non-Newtonian Fluid Mech. **129**, 1 (2005).
[2] A. Groisman and V. Steinberg, Nature (London) **405**, 53 (2000).
[3] A. Groisman and S. R. Quake, Phys. Rev. Lett. **92**, 094501 (2004).
[4] A. Karnis, S. Mason, and H. Goldsmith, Nature (London) **200**, 159 (1963).
[5] A. Karnis, H. Goldsmith, and S. Mason, Can. J. Chem. Eng. **44**, 181 (1966).
[6] B. Ho and L. Leal, J. Fluid Mech. **65**, 365 (1974).
[7] F. Gauthier, H. L. Goldsmith, and S. Mason, Rheol. Acta **10**, 344 (1971).
[8] F. Gauthier, H. Goldsmith, and S. Mason, Trans. Soc. Rheol. **15**, 297 (1971).
[9] B. Ho and L. Leal, J. Fluid Mech. **76**, 783 (1976).
[10] S. Dhahir and K. Walters, J. Rheol. (N.Y.) **33**, 781 (1989).
[11] E. Carew and P. Townsend, Rheol. Acta **30**, 58 (1991).
[12] P. Huang, J. Feng, H. H. Hu, and D. Joseph, J. Fluid Mech. **343**, 73 (1997).
[13] A. Karnis and S. G. Mason, J. Colloid Interface Sci. **24**, 164 (1967).
[14] P.-H. Chan and L. Leal, Int. J. Multiphase Flow **7**, 83 (1981).
[15] M. King and D. Leighton, Phys. Fluids **13**, 397 (2001).
[16] S. Hudson, Phys. Fluids **15**, 1106 (2003).
[17] K. Hollingsworth and M. Johns, J. Colloid Interface Sci. **296**, 700 (2006).
[18] P.-H. Chan and L. G. Leal, J. Fluid Mech. **92**, 131 (1979).
[19] T. Beatus, T. Tsulty, and R. Bar-Ziv, Nature Phys. **2**, 743 (2006).
[20] S. L. Anna, N. Bontoux, and H. A. Stone, Appl. Phys. Lett. **82**, 364 (2003).
[21] P. Garstecki, I. Gitlin, W. DiLuzio, G. M. Whitesides, E. Kumacheva, and H. A. Stone, Appl. Phys. Lett. **85**, 2649 (2004).